Electronic Supplementary Material (ESI) for Journal of Materials Chemistry A.

Supplementary Information

Ion Transport through Layered Hydrogels for Low-Frequency Energy Harvesting toward Self-Powered Chemical Systems

Merreta Noorenza Biutty[1,†], Ja-Min Koo[1,†], Joo Hyun Kim[1], Seonho Kim[2], U Hyeok Choi[2], Kusuma Betha Cahaya Imani[3], Jinhwan Yoon[3], Byoung-Yong Chang[4], and Seong Il Yoo[1,*]

[1]Department of Polymer Engineering, Pukyong National University, Busan 48547, Korea
Email: siyoo@pknu.ac.kr; Tel: +82-51-629-6456

[2]Department of Polymer Science and Engineering and Program in Environmental and Polymer Engineering, Inha University, Incheon 22212, Korea

[3]Graduate Department of Chemical Materials, Pusan National University, Busan, 46241, Korea

[4]Department of Chemistry, Pukyong National University, Busan 48547, Korea

[†]These authors contributed equally to this work.

When the PAAm(S) (or PAAm(H)) hydrogels with 2.0 M of [NaCl] was stacked with PAAc hydrogels without NaCl, the stacked PAAm(S)/PAAc (or PAAm(H)/PAAc) hydrogels exhibited an intermediate conductivity.

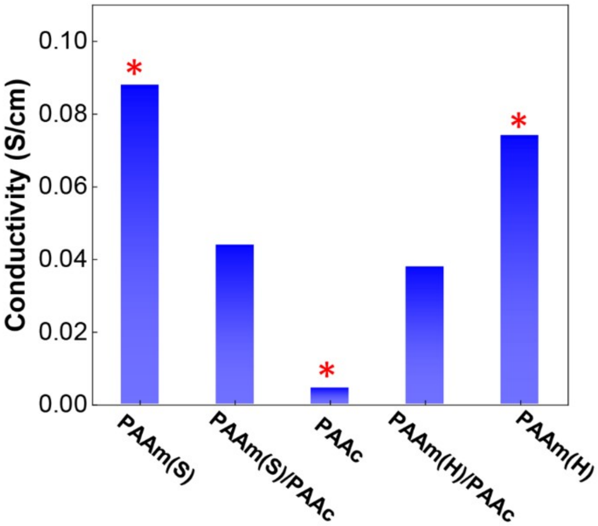

Figure S1. Ion conductivities of various hydrogels with different configurations. The concentration of NaCl was set as 2.0 M for both the PAAm(S) and PAAm(H) hydrogels, and as zero for the PAAc hydrogel. The component PAAm(S), PAAm(H), and PAAc hydrogels are marked with an asterisk (*).

When the device with 12-mm-thick PAAm(S)/PAAc/PAAm(H) hydrogels was compressed to a different degree, the electric outputs increased with the compressional thickness (Figure S2a and S2b). In the next step, the thickness of the stacked hydrogels was increased to 24 mm by doubling the thicknesses of all the component hydrogels. Then, the device with 24-mm-thick hydrogels was compressed to further study the influence of the thickness (Figure S2c and S2d). Even though both the total thickness and the degree of compression were doubled, the electric performance of the device was not improved but worsened. It appears that, as the thickness of the hydrogel increases, the steric effect for the ions during transporting through the hydrogels also increases; this might perturb the directional ion transport, resulting in the worsened electric performance. Based on the result, we maintained the thickness of PAAm(S)/PAAc/PAAm(H) hydrogels as 12 mm throughout this study.

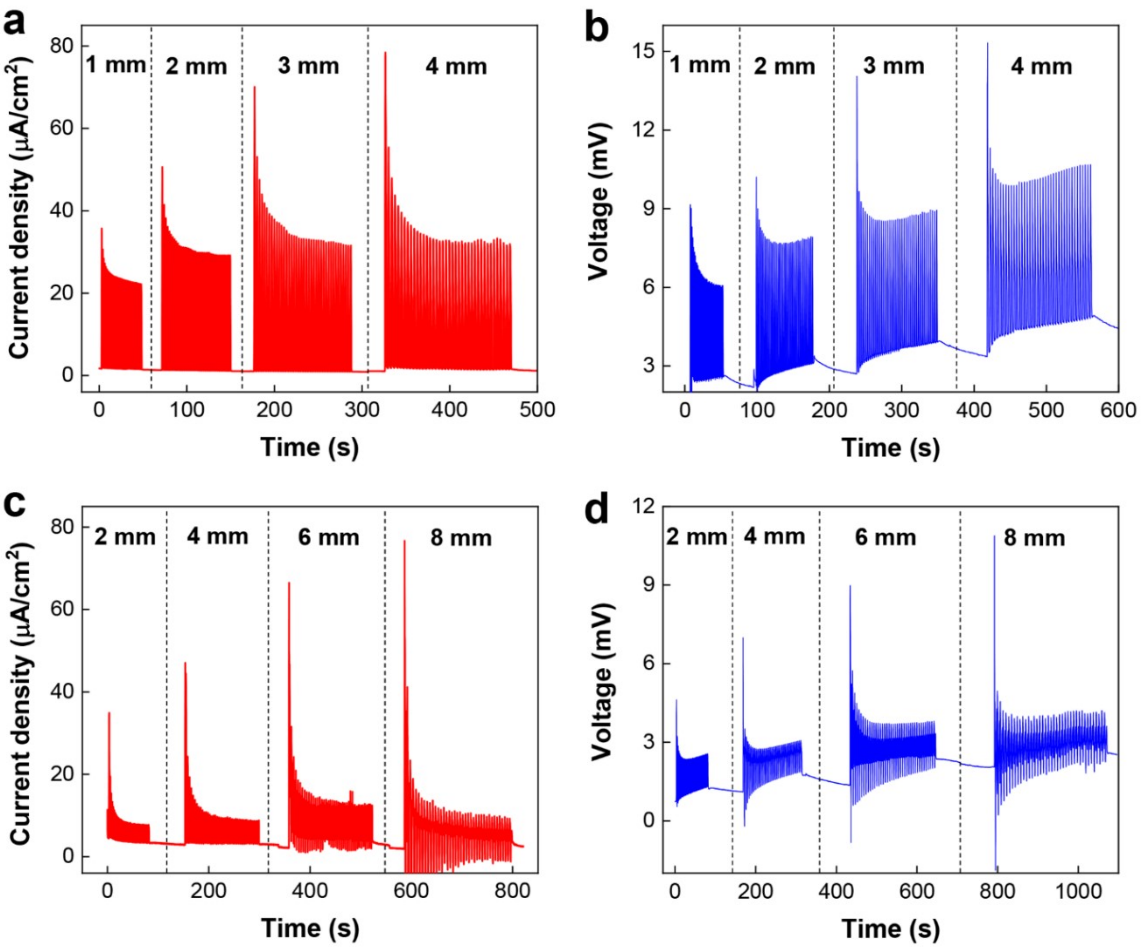

Figure S2. (a, c) Short-circuit current densities and (b, d) open-circuit voltages obtained for the devices composed of (a, b) 12-mm- and (c, d) 24-mm-thick stacked PAAm(S)/PAAc/PAAm(H) hydrogels with under different compressional thicknesses.

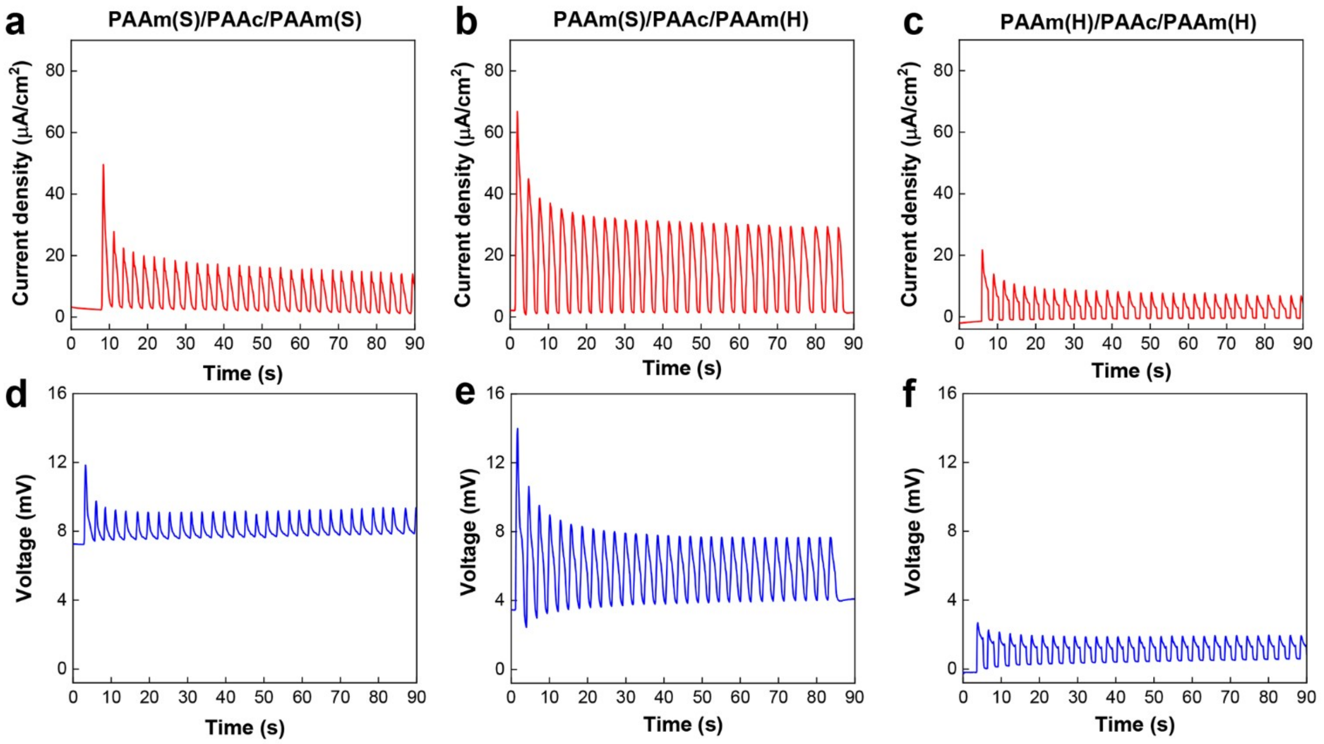

Figure S3. (a–c) Short-circuit current densities and (d–f) open-circuit voltages for the devices prepared using the various stacked hydrogels: (a, d) PAAm(S)/PAAc/PAAm(S); (b, e) PAAm(S)/PAAc/PAAm(H); and (c, f) PAAm(H)/PAAc/PAAm(H).

In this set of experiments, the amount of the MBAA (crosslinker) in the monomeric solution was adjusted to study the effect of the stiffness of the hydrogels. Here, it needs to be noted that 10 and 250 mg of MBAA, which were used for the preparation PAAm(S) and PAAm(H) hydrogels in the main text, can be considered as the lower and upper limits. For instance, when the amount of MBAA was larger than 250 mg, the hydrogel became fragile and was easily destructed under the continued compression-release cycles. In contrast, when the amount of crosslinker was smaller than 10 mg, the electric outputs from the hydrogel device became unstable, and the measured values were different at each sample preparation. In this regard, we fixed the amount of MBAA as 250 mg for PAAm(H), and increased the amount of MBAA for PAAm(S) hydrogels above 10 mg. By comparing this result in Figure S4, it can be validated that the inhomogeneous compression of the PAAm(S) and PAAm(H) layers has been optimized in the main text.

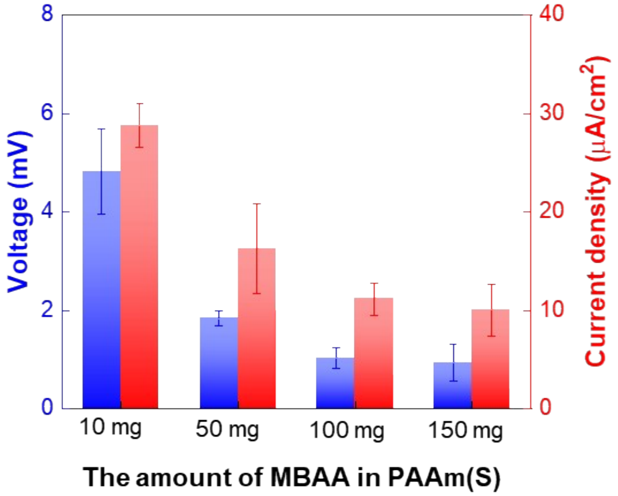

Figure S4. Open-circuit voltages (blue) and short-circuit current densities (red) of the device prepared using PAAm(S)/PAAc/PAAm(H) hydrogels. The amount of MBAA in the PAAm (S) hydrogels was adjusted as 10 – 150 mg, while that in the PAAm (H) hydrogel was fixed as 250 mg.

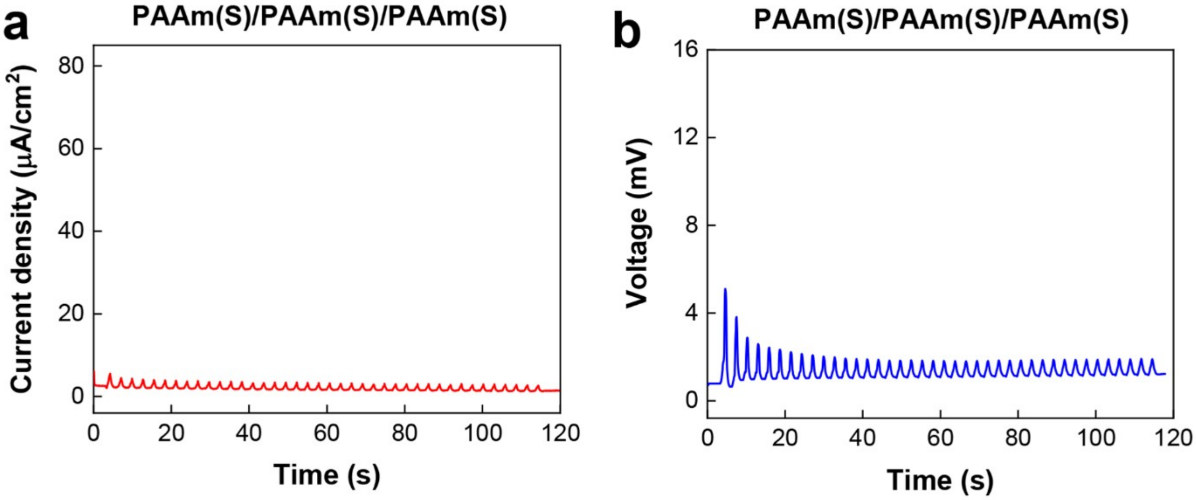

Figure S5. (a) Short-circuit current densities and (b) open-circuit voltages for the devices based on PAAm(S)/PAAm(S)/PAAm(S) hydrogels.

Since the mechanical properties of the PAAc hydrogel worsened with increasing pH, we increased the amount of crosslinker (MBAA) in the monomeric solution to 120 mg (typically 20 mg of MBAA was utilized for the uncontrolled hydrogel in the main text). This may reduce the current density of the hydrogel device before the addition of NaOH(s) (see Figure S6a). With an increase in the pH, both the V_{OC} and I_{SC} values increased, as shown in Figure S6e.

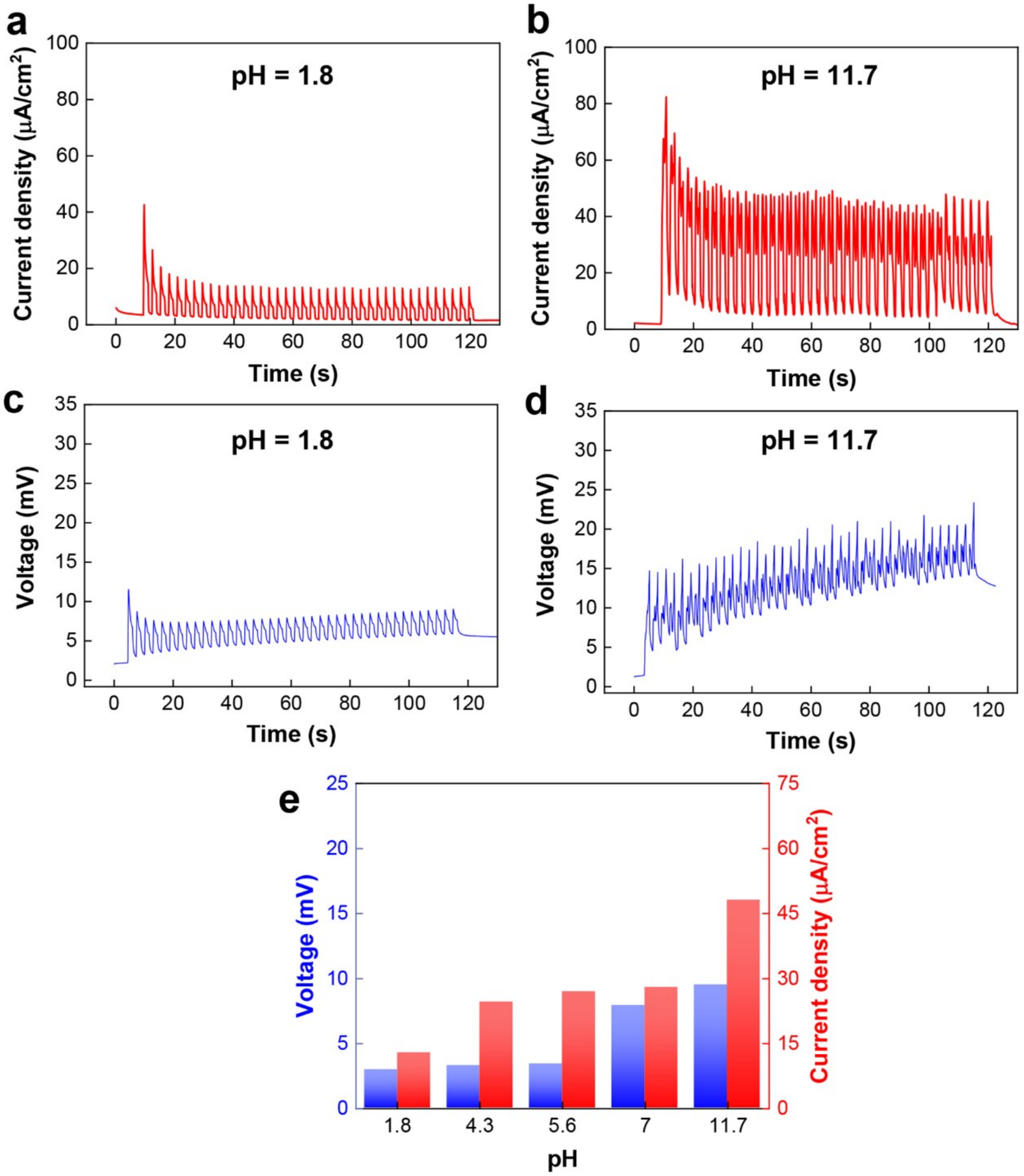

Figure S6. (a, b) Short-circuit current densities and (c, d) open-circuit voltages for the device based on PAAm(S)/PAAc/PAAm(H) hydrogels, wherein the pH of the PAAc hydrogel was controlled. (a, c) pH = 1.8 and (b, d) pH = 11.7. (e) Output performances of the same device under various pH conditions. The pH of PAAc hydrogel was adjusted by adding NaOH(s) to the acrylic acid monomer solution.

To prepare other types of cation-selective hydrogels, the PAAm hydrogel was blended with charged polyelectrolytes. For this purpose, poly(sodium 4-styrenesulfonate, PSS) (Mw = 70,000 g/mol), sodium polyacrylic acid (PSA) (Mw = 15,000 g/mol), and crystalline nanocellulose (CNC) were selected, the molecular structures of which are shown in scheme S1. To prepare the blended hydrogel, the AAm monomer (3 g) and the MBAA crosslinker (30 mg) were dissolved in PSS, PSA, or CNC (12 mL). The amount of the polyelectrolyte was adjusted with respect to the mass of DI water, i.e., 7 wt% for PSS, 7 wt% for PSA, and 1.5 wt% for CNC. The monomeric solution was then degassed in a vacuum oven at 60 °C for 30 min and then cooled to room temperature. Subsequently, an aliquot (100 µL) of an aqueous APS solution (initiator) and TEMED (10 µL, catalyst) was added to the solution. The reaction mixture was quickly cast into a round-shaped glass mold with an inner diameter of 36.5 mm and a thickness of 4 mm. Polymerization was carried out at 40 °C for 30 min after covering the molds.

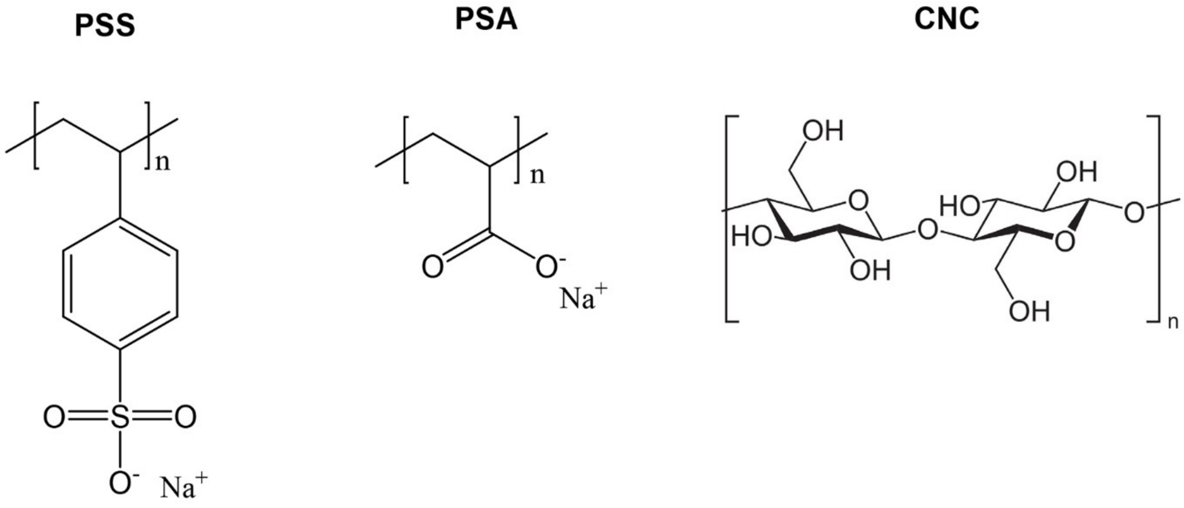

Scheme S1. Molecular structures of PSS, PSA, and CNC

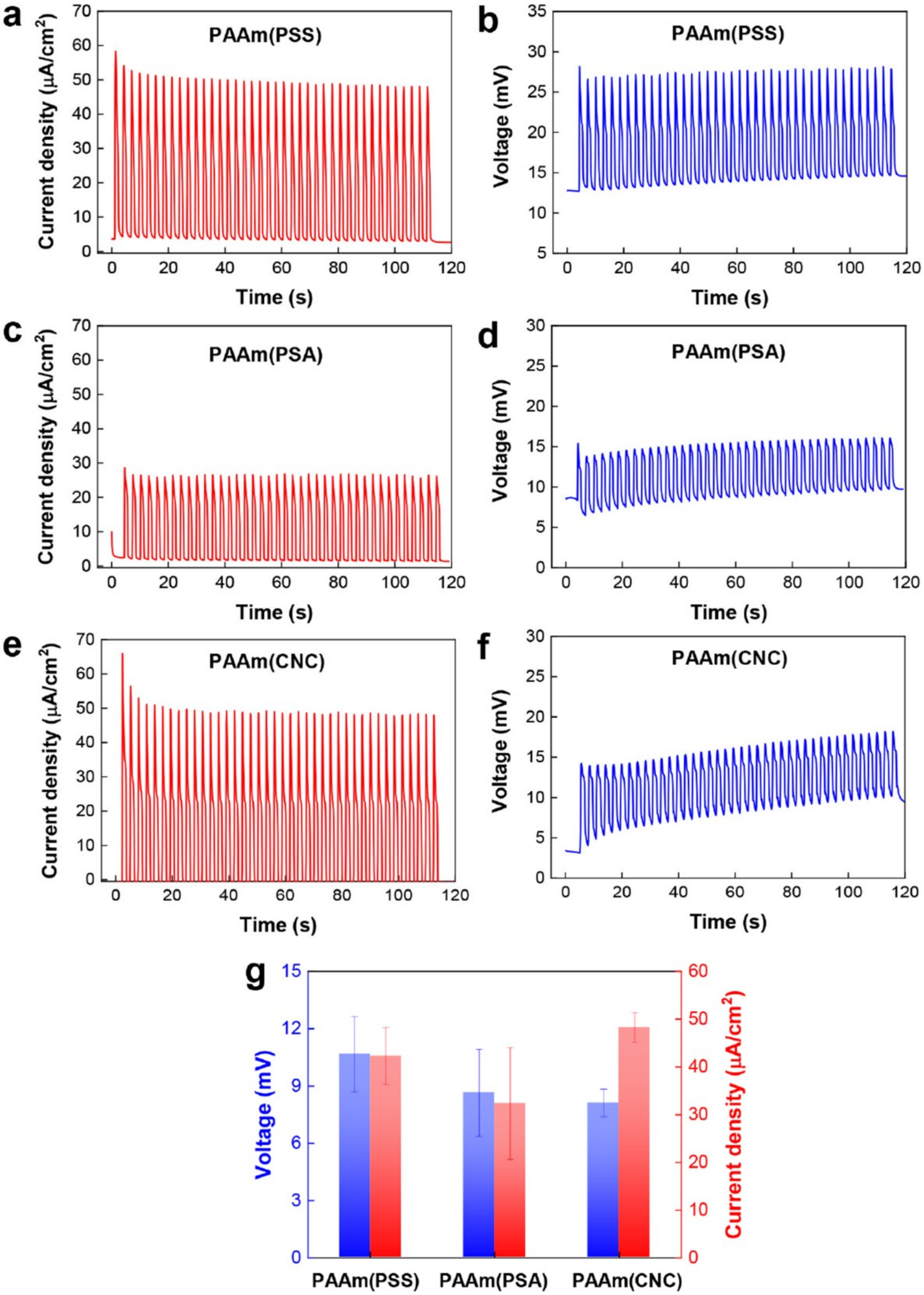

Figure S7. (a, c, e) Short-circuit current densities and (b, d, f) open-circuit voltages for the hydrogel devices prepared using other types of cation-selective hydrogels. (a, b) PAAm (PSS); (c, d) PAAm (PSA); and (e, f) PAAm (CNC). (g) The average electrical outputs from hydrogel devices using different types of cation-selective hydrogels.

The specific capacitance as a function of angular frequency and the corresponding average capacitance at $\omega = 1$ rad/s (after an electrical double layer (EDL) formation) and $\omega = 10^5$ rad/s (before EDL formation) for hydrogels-based ionic conductors in successive compression and release cycles are displayed in Figure S8. The specific capacitance shown at low frequencies is associated with the EDL capacitance. In Figure S8a and its inset, it is clear that the compression leads to a significant increase in the capacitance value from ~200 μF/cm^2 at $\omega = 1$ rad/s (initial state) to ~1000 μF/cm^2 at $\omega = 1$ rad/s (1st compressed state). Upon releasing the compression, the capacitance was restored to the initial value. This pressure-sensitive EDL capacitance was still present after multiple compression and release cycles (see Figure S8b). Interestingly, even at high frequencies ($\omega = 10^5$ rad/s, before EDL formation), the specific capacitance of hydrogel ionic conductor exhibited the same compressive dependence (Figure S8c); the capacitance values in the compressed state were higher than those in the released state.

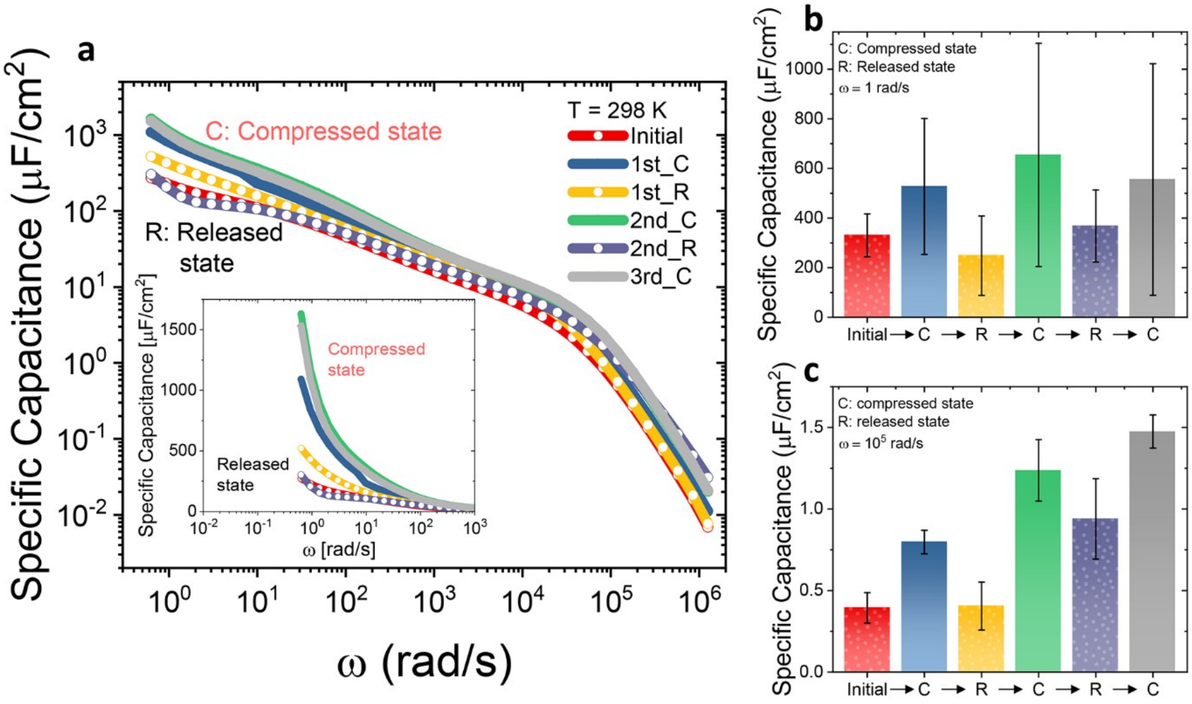

Figure S8. (a) Representative specific capacitance as a function of angular frequency ω at 298 K for a hydrogel-based ionic conductor in successive compression and release cycles. Comparison of specific capacitance at (b) $\omega = 1$ rad/s and (c) $\omega = 10^5$ rad/s for continuous compressed and released sample in capacitor, where error bars show standard deviation; sample size $N = 3$.

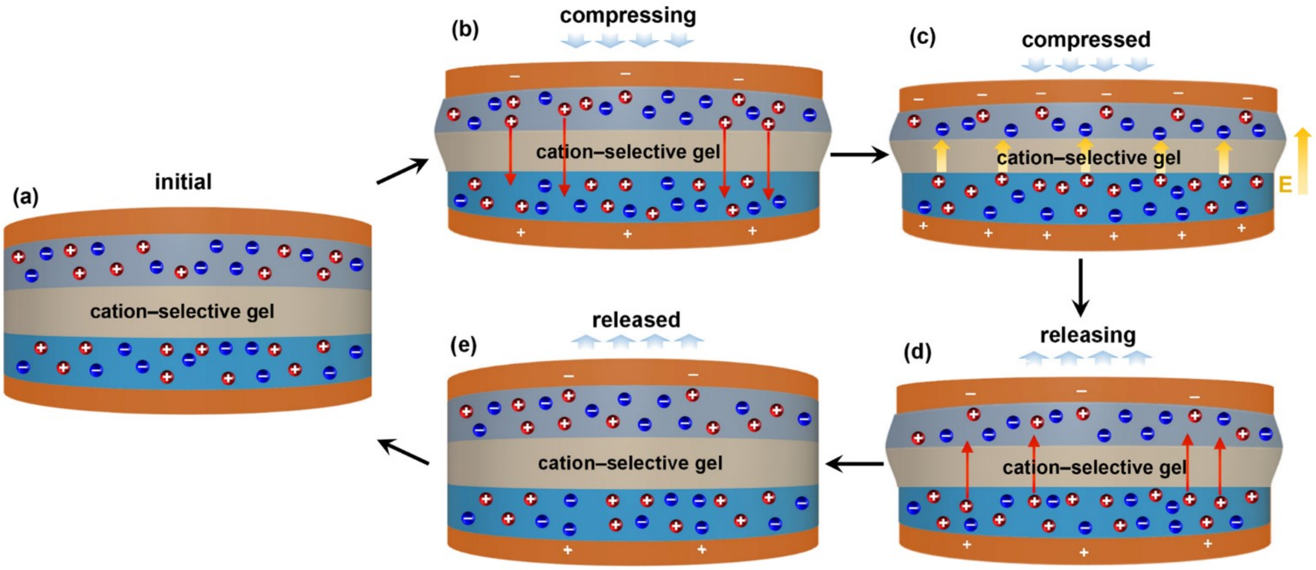

Scheme S2. Schematic illustration of energy-harvesting procedure in the hydrogel device: (a) Initial state. (b) The transport of cations from the top PAAm(S) to the bottom PAAm(H) hydrogels upon compression. (c) The development of electric field from PAAm(H) to PAAm(S) hydrogels with the formation of EDL. (d) The transport of cations from the bottom PAAm(H) to the top PAAm(H) hydrogels upon release. (e) Redistribution of ions to the homogenous state with the disappearance of EDL.

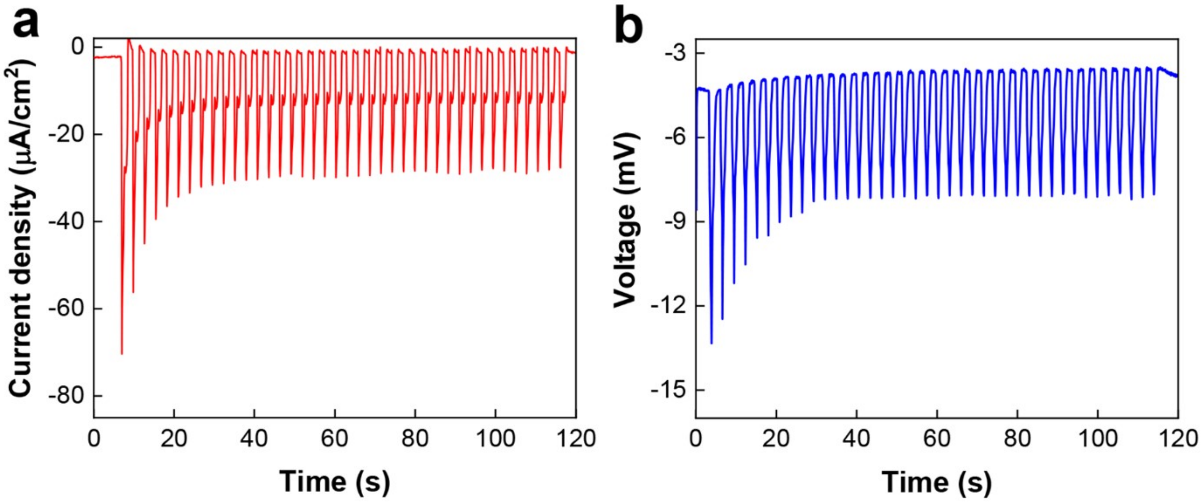

Figure S9. (a) Short-circuit current density and (b) open-circuit voltage for the device prepared using the PAAm(S)/PAAc/PAAm(H) hydrogels under reversed polarity connection conditions.

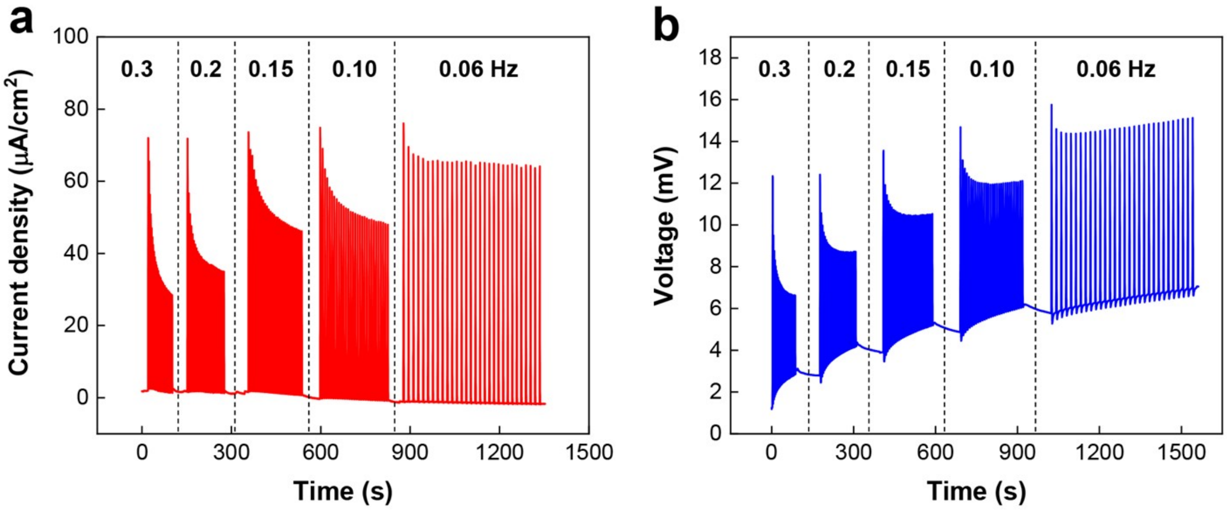

Figure S10. (a) Short-circuit current density and (b) open-circuit voltage of the device prepared using the stacked PAAm(S)/PAAc/PAAm(H) hydrogels under different vibrational frequency conditions.

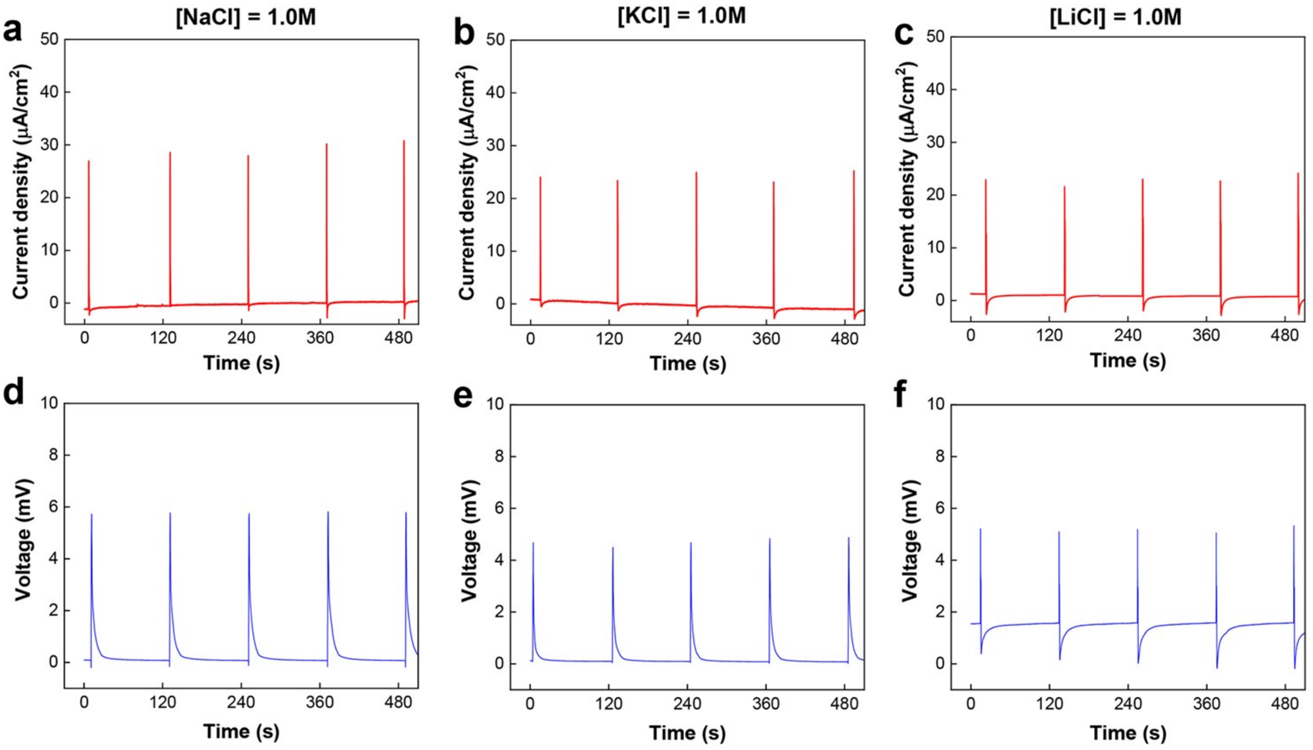

Figure S11. (a–c) Short-circuit current densities and (d–f) open-circuit voltages for the device prepared using the stacked PAAm(S)/PAAc/PAAm(H) hydrogels at a vibrational frequency of 0.008 Hz. The electrolytes examined were (a, d) NaCl, (b, e) KCl, and (c, f) LiCl.

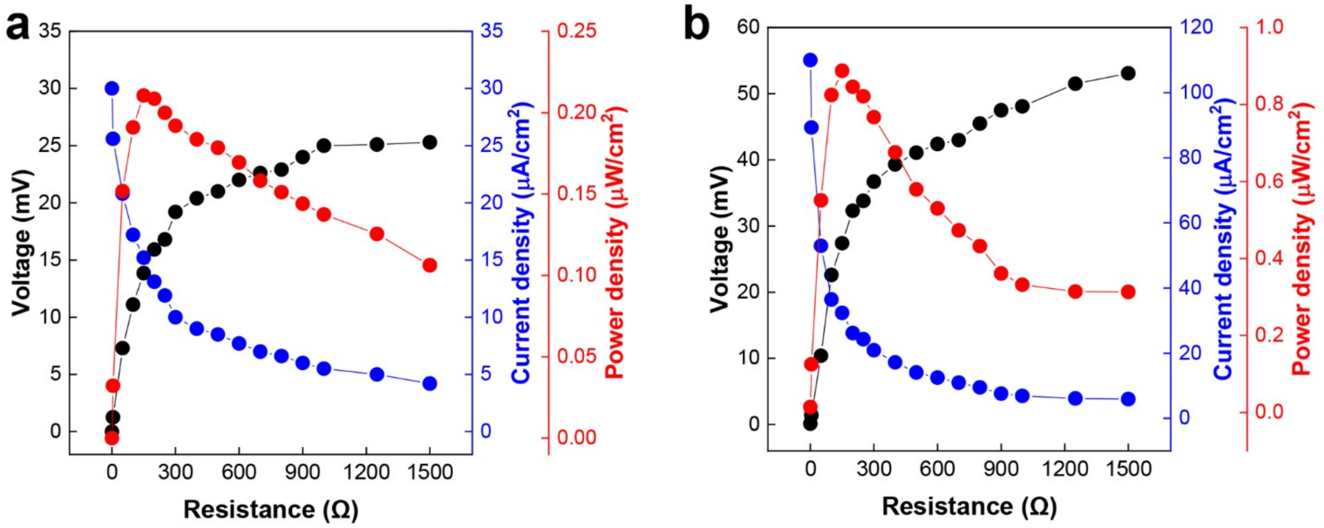

Figure S12. Output voltages (black), current densities (blue), and power densities (red) of the hydrogel devices containing 4 cells of PAAm(S)/PAAc/PAAm(H) connected in series. The vibrational frequency was set as (a) 0.3 Hz and (b) 0.008 Hz.

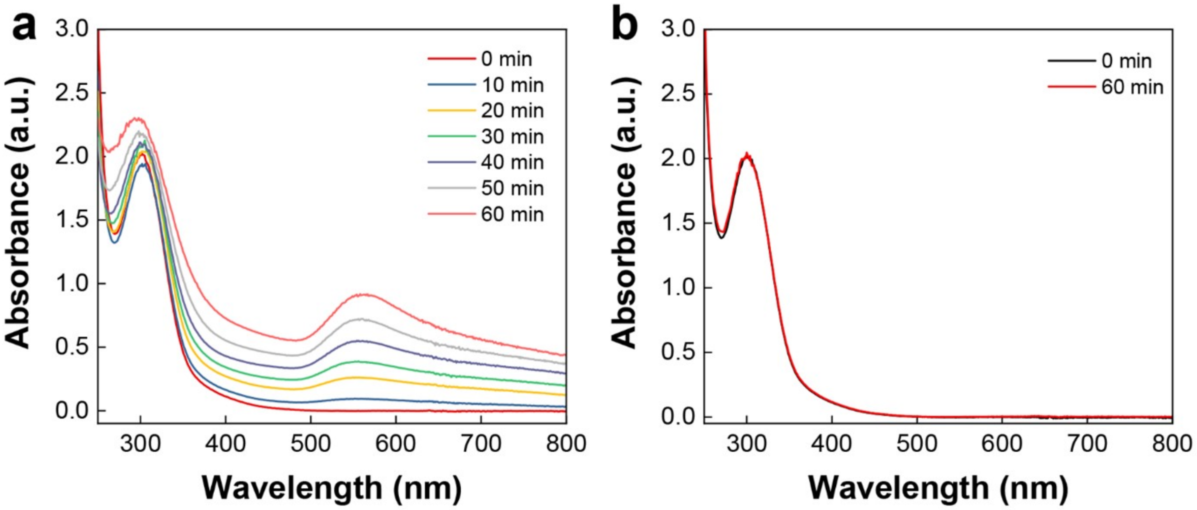

Figure S13. UV-Vis spectra of the aqueous solution of $HAuCl_4$: (a) connected with power supply with output voltage of 5.0 mV; (b) connected with the hydrogel devices but without compression-release procedures.

As found in the TEM image with elementary maps (Figure S14), the polyhedral Au nanoparticles were synthesized by the cell-potential produced from the hydrogel device. The cell-potential was 4.6 mV. Note, this voltage is not sufficient to drive faradaic reactions in Figure S15a, where two Pt electrodes were immersed in the electrolyte containing $AuCl_4^-$. However, when one of the two Pt electrodes was replaced with an easily oxidizable tin-coated copper electrode, the small cell-potential became able to drive faradaic reactions (Figure S15b). Remember that the standard reduction potential of tin is very low: $Sn^{2+}(aq) + 2e \rightarrow Sn(s)$ at -0.1375 V vs. SHE. The oxidized tin, Sn^{2+}, can be oxidized further as its reduction potential is still lower than reduction of $AuCl_4^-$

$$Sn^{4+}(aq) + 2e \rightarrow Sn^{2+}(aq) \text{ at } 0.15 \text{ V vs. SHE}$$

$$AuCl_4^- + 3e \rightarrow Au(s) + 4Cl^- \text{ at } 0.994 \text{ V vs. SHE.}$$

As a result, the oxidized tin plays a role of the reducing agent for $AuCl_4^-$. It is strongly supported by the observation that Au nanoparticles were produced in the bulk instead of being deposited on the electrode. Synthesis of Au nanoparticle using reducing agents is very well-known process and reported in the many literatures.

In this study, we utilized tin-coated copper wire, which contained small amount of Fe (see EDS spectrum of Figure S16). Fe blended in the tin-coated copper wire electrode took similar process. When the electrode undergoes the oxidation reaction, not only Sn but Fe also oxidized: $Fe^{2+}(aq) + 2e \rightarrow Fe(s)$ at -0.44 V vs. SHE. Then, the oxidized iron forms iron oxide and co-deposited on the Au nanoparticle when Sn^{2+} reduces $AuCl_4^-$ as shown in Figure S14b.

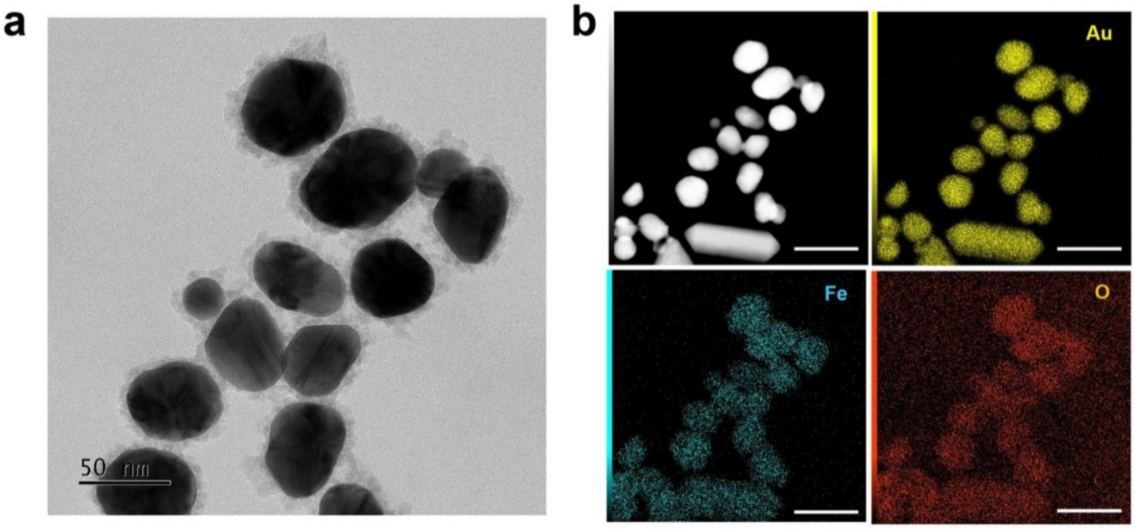

Figure S14. (a) TEM and (b) STEM image of Au-iron oxide nanoparticles with EDS maps. EDX elemental maps of Au, Fe, and O are colored in yellow, blue, and red, respectively. The scale bar in the images corresponds to 100 nm.

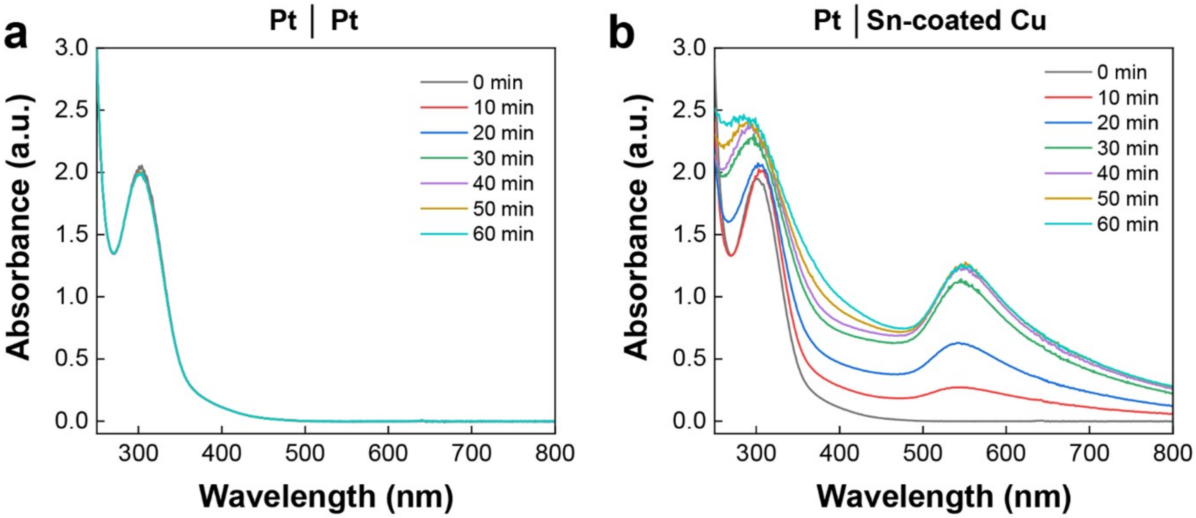

Figure S15. UV-Vis spectra of the aqueous solution of $HAuCl_4$ connected with the hydrogel devices with continued compression-release cycles at 0.3 Hz. The two Cu electrodes of hydrogel device were connected to the $HAuCl_4$ solution by (a) two Pt wires and (b) Pt and Sn-coated Cu wires.

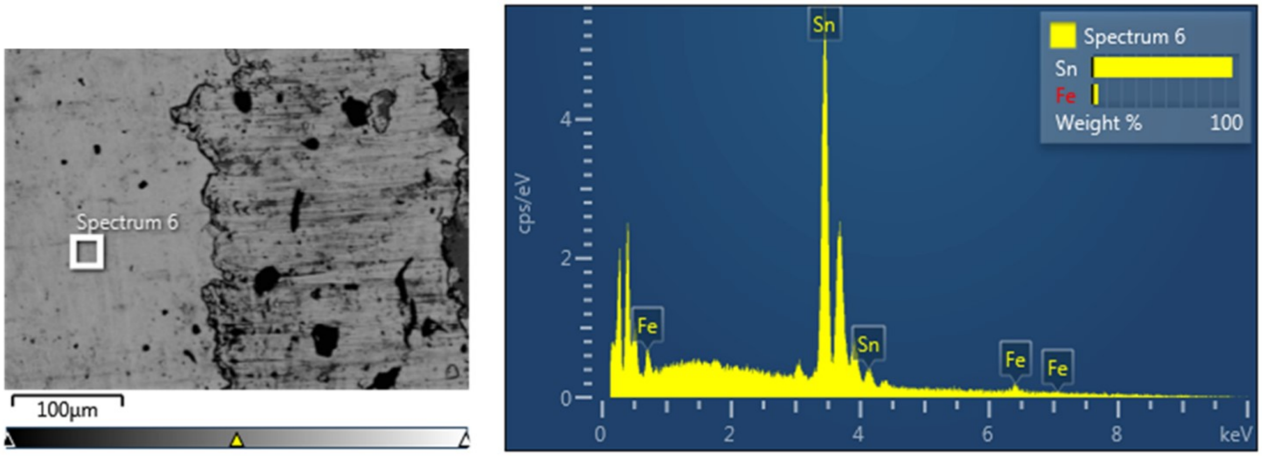

Figure S16. EDS spectrum of tin-coated copper wire from the boxed region in the SEM image.